Cardiac metabolic effects of $K_{Na}1.2$ channel deletion, and evidence for its mitochondrial localization.

Charles O. Smith[1], Yves T. Wang[2], Sergiy M, Nadtochiy[2], James H. Miller[2], Elizabeth A. Jonas[3], Robert, T. Dirksen[4], Keith Nehrke[4,5], Paul S. Brookes[2,4,*]

From: Departments of [1]Biochemistry, [2]Anesthesiology and Perioperative Medicine, [4]Pharmacology & Physiology, [5]Medicine, University of Rochester Medical Center, Rochester, NY 14642, USA. [3]Department of Internal Medicine, Section of Endocrinology, Yale University School of Medicine, New Haven, CT 06511, USA.

*To whom correspondence should be addressed:

Paul S. Brookes, PhD.
Department of Anesthesiology, Box 604,
University of Rochester Medical Center,
601 Elmwood Avenue,
Rochester, NY 14642, USA.
paul_brookes@urmc.rochester.edu
Tel… 585-273-1626

Running title: *Cardiac Mitochondria & $K_{Na}1.2$*

Non-standard abbreviations

IR injury: Ischemia-Reperfusion injury

IPC: Ischemic Preconditioning

APC: Anesthetic Preconditioning

K_{Na}: Sodium activated potassium channel

$K_{Na}1.1$ (channel encoded by *Kcnt1* (formerly Slo2.2)), aka Slack, $K_{Ca}4.1$, SLO2.2

$K_{Na}1.2$ (channel encoded by *Kcnt2* (formerly Slo2.1)), aka Slick, $K_{Ca}4.2$, SLO2.1

BT: Bithionol, aka Bis(2-hydroxy-3,5-dichlorophenyl)Sulfide

OCR: Oxygen consumption rate

ROS: Reactive oxygen species

Abstract

Controversy surrounds the molecular identity of mitochondrial K^+ channels that are important for protection against cardiac ischemia-reperfusion injury. While $K_{Na}1.2$ (*Kcnt2* gene) is necessary for cardioprotection by volatile anesthetics, electrophysiologic evidence for a channel of this type in mitochondria is lacking. The endogenous physiologic role of a potential mito-$K_{Na}1.2$ channel is also unclear. Herein, single channel patch-clamp of 27 independent cardiac mitochondrial inner membrane (mitoplast) preparations from wild type (WT) mice yielded 6 channels matching the known ion-sensitivity, ion-selectivity, pharmacology and conductance properties of $K_{Na}1.2$ (slope conductance 138±1 pS). However, similar experiments on 40 preparations from *Kcnt2*$^{-/-}$ mice yielded zero such channels. The K_{Na} opener bithionol uncoupled respiration in WT but not *Kcnt2*$^{-/-}$ cardiomyocytes. Furthermore, when oxidizing only fat as substrate, *Kcnt2*$^{-/-}$ cardiomyocytes and hearts were less responsive to increases in energetic demand. *Kcnt2*$^{-/-}$ mice also had elevated body fat, but no baseline differences in the cardiac metabolome. These data support the existence of a cardiac mitochondrial $K_{Na}1.2$ channel, and a role for cardiac $K_{Na}1.2$ in regulating metabolism under conditions of high energetic demand.

Key words: Patch Clamp, Slick, Slo2.1, Bithionol

Introduction

Numerous strategies for protection of the heart and other organs against ischemia-reperfusion (IR) injury are thought to require activation of K^+ channels in the mitochondrial inner membrane (for review see (1)). This includes ischemic preconditioning (IPC), volatile anesthetic preconditioning (APC), and pharmacologic cardioprotection by K^+ channel activators such as NS-11021, bithionol and diazoxide (2–4). Concurrently, several K^+ channels have been reported in mitochondria including: ATP activated (K_{ATP}) (5), small conductance Ca^{2+} activated (SK) (6, 7), and splice variants of large conductance Ca^{2+} activated (BK) (8, 9). However, in only a small number of cases has the molecular (genetic) identity of specific mitochondrial channels involved in cardioprotection been proposed (3, 9–12). No K^+ channels exist in the "MitoCarta" database of verified mitochondrial proteins (13) and no canonical mitochondrial target sequences have been identified in any K^+ channel genes (1). As such, mystery surrounds the mechanism(s) of K^+ channel targeting to mitochondria.

Mammalian Na^+-activated-K^+ (K_{Na}) channels are encoded by two genes: *Kcnt1* (14) and *Kcnt2* (15), which produce the $K_{Na}1.1$ (Slack/SLO2.2) and $K_{Na}1.2$ (Slick/SLO2.1) channels respectively. Both $K_{Na}1.1$ and $K_{Na}1.2$ channels play important neurologic roles in the termination of seizure progression in epilepsy (16, 17). Although $K_{Na}1.2$ expression has been reported in cardiac tissue (15, 18), and a generic K_{Na} channel activity has been demonstrated in the cardiac cell membrane (19), notably the *Kcnt2*$^{-/-}$ mice have no cardiac phenotype (3, 18). Thus relatively little is known regarding the physiologic role of $K_{Na}1.2$ channels in the heart, including their subcellular location. Previously we showed that $K_{Na}1.2$ is essential for cardiac APC, with hearts from *Kcnt2*$^{-/-}$ mice incapable of being protected against IR injury by isoflurane (3). Additionally, we showed that the K_{Na} opener bithionol (BT) is cardioprotective in WT mice but not *Kcnt2*$^{-/-}$ mice (3, 20). Further, both BT and isoflurane activated a K^+ flux in cardiac mitochondria isolated from WT mice, but not those from *Kcnt2*$^{-/-}$ mice (3). These observations led us to hypothesize that a $K_{Na}1.2$ channel may exist in cardiac mitochondria.

There is considerable evidence that mitochondrial K^+ channel activity can lessen the impact of IR injury (1). less is known about the endogenous physiologic role(s) of mitochondrial K^+ channels (21), and in particular mitochondrial K_{Na} channels. Na^+ enters mitochondria predominantly via a Na^+/Ca^{2+} exchanger (NCLX) or a Na^+/monocarboxylate transporter (MCT), with minor contribution from a Na^+/H^+ exchanger (NHE) (22). Under conditions of elevated mitochondrial Na^+ uptake (Ca^{2+} overload or cytosolic Na^+ overload driving excessive NCLX activity, or increased cytosolic Na^+-lactate driving Na^+ uptake via the MCT), matrix Na^+ may attain levels that can activate K_{Na} channels (23–25). K^+ influx via the K_{Na} would dissipate mitochondrial membrane potential, thereby relieving a driving force both for Ca^{2+} uptake and NCLX activity. In effect, a mitochondrial K_{Na} channel acts as a "safety valve" to prevent ionic imbalance bought about by excessive Na^+ uptake.

Herein, using electrophysiologic techniques (mitoplast patch-clamp) we demonstrate that mitochondria contain a K^+ channel that matches the known ion-sensitivity, ion-selectivity, pharmacology and conductance

properties of $K_{Na}1.2$. Bioenergetic studies of WT and *Kcnt2*$^{-/-}$ hearts and cardiomyocytes also reveal a potential role for cardiac $K_{Na}1.2$ in the metabolic response to high energetic demand.

Materials and Methods

Animals

Male and female mice were housed in an AAALAC-accredited pathogen-free facility with water and food available *ad libitum*. All procedures were locally approved and in accordance with the NIH *Guide for the Care and Use of Laboratory Animals* (2011 revision). Mice were on a C57BL/6J background for >6 generations and periodically backcrossed to fresh stocks. Mice were bred from *Kcnt2*$^{+/-}$ parents, and male and females were separated but littermate WT and *Kcnt2*$^{-/-}$ progeny were maintained in the same cages. Mice were genotyped by tail-clip PCR (Figure 1A), with DNA extraction by a Qiagen DNeasy™ Kit (Hilden, Germany) and genotyping by a Kapa Biosystems KAPA2G Kit (Wilmington, MA). Primers used were (5'→3') forward-AGGCAGCCATAGCTTTAGAGA and reverse CTCCTCATCGTGTGGTCCTA, yielding amplicons at 822 and 547 bp for WT and *Kcnt2*$^{-/-}$ respectively. Due to the same personnel handling mice and performing experiments, studies were not blinded to genotype.

Patch Clamp of Mitochondrial Inner Membranes (Mitoplasts)

Following anesthesia (tribromoethanol 200mg/kg ip) the heart from one 8-12 week old mouse was rapidly excised, washed and chopped in ice-cold mitochondrial isolation medium (MIM, in mM: 300 sucrose, 20 Tris, 2 EGTA, pH 7.35 at 4 °C). All steps were performed on ice. Tissue was homogenized (Tissumizer™, IKA Inc., Wilmington NC) then centrifuged at 700 x *g*, 5 min. Supernatants were saved and pellets re-homogenized and re-centrifuged. Pooled supernatants were then centrifuged at 10,000 x *g*, 10 min. The crude mitochondrial pellet was suspended in 0.2 ml MIM and layered over 1.75 ml of 30% osmotically-balanced Percoll™, in a round-bottomed microcentrifuge tube, and centrifuged at 14,000 x *g*, 1 hr. Two mitochondrial layers were apparent (Figure 1C), of which the lower (purified mitochondria) was washed twice by centrifugation. The mitochondrial pellet (~25 µl) was suspended in 0.5 ml swelling buffer (in mM: 30 KCl, 20 HEPES, 1 EGTA, pH 7.2) for 15 min. Centrifugation (1,000 x *g*, 30 s.) afforded a mitoplast pellet, resuspended in ~20 µl MIM for immediate use in patch-clamp studies (N=27 WT, 40 *Kcnt2*$^{-/-}$).

For mitoplast attached patch-clamp studies, mitoplasts were diluted 1:100 in a bath solution (in mM: 150 KCl, 20 HEPES, 1 EGTA, pH 7.2) and a 10 µl drop was placed on a glass coverslip attached to a custom 3D printed micro-chamber (Figure 1B). Electrodes (40-100 M→) (Sutter Instruments, Novato CA) were filled with pipette solution (in mM: 150 KCl, 0.025 NaCl, 20 HEPES, 1 EGTA, pH 7.2). The bath was exchanged with buffer additionally containing 40 mM NaCl, or 40mM NaCl and 10 µM bithionol (BT, from stock in DMSO,

final DMSO < 0.01% v/v). For excised patch experiments mitoplasts were diluted 1:100 in patch seal buffer (in mM: 60 KCl, 80 K-gluconate, 40 LiCl, 0.025 NaCl, 0.1 $CaCl_2$ (calculated free), 20 HEPES, 1 EGTA, pH 7.2) Electrodes were filled with pipette solution (in mM: 125 KCl, 15 K-gluconate, 15 LiCl 0.025 NaCl, 20 HEPES, 1 EGTA). Mitoplasts were identified by their round shape and presence of a "cap" structure (Figure 1C). After formation of G→seals, patches were excised and inside-out currents were recorded using an Axopatch 200B amplifier and Clampex10 software (Molecular Devices, Sunnyvale CA). All holding potentials reported are those applied to the patch pipette interior. The electrical connection was made using Ag/AgCl electrodes and an agar 2M KCl salt bridge at the ground electrode. (Note: not all channels yielded currents at all potentials, and seal integrity was often compromised at the extremes of this range). Data was digitized and recorded at 10 kHz and filtered using an 8-pole low pass 2 kHz filter. Patches were recorded under flow (0.1 ml/min.) of: (i) Ca^{2+} free patch seal buffer with 0.076 mM sucrose for osmotic balance, (ii) as above, with LiCl replaced with 40 mM NaCl, (iii) further addition of 2.5 µM BT (from stock in DMSO, final DMSO < 0.01% v/v). Although the study of K^+ channels typically employs gluconate salts to exclude the possibility that measured conductances are due to Cl^- channels, Cl^- salts were used herein because $K_{Na}1.2$ activity is strongly enhanced in the presence of Cl^- (15). All buffers were filtered (0.22 µm) immediately before use. Single channel analysis was performed using Clampfit 10.0 single channel search (Molecular Devices). Dwell times were calculated using "single-channel search" using threshold crossing.

Cardiomyocyte Isolation and Respiration Measurements

Mouse primary adult ventricular cardiomyocytes were isolated by collagenase perfusion as previously described (3). Cells were step-wise rendered tolerant to 1.8 mM Ca^{2+}, and the final pellet suspended in 1 ml MEM (GIBCO cat # 11095-080, supplemented with 1.8 mM, $CaCl_2$ 2.5% FBS and pen/strep). Cell viability and yield were determined using Trypan blue and a hemocytometer. Only preparations with >85% viable rod-shaped cells were used for experiments. Cells were seeded at 2000/well on Seahorse™ XF96 V3-PS plates (Agilent, Billerica MA) and equilibrated for 1 hr. MEM was replaced with unbuffered DMEM (pH 7.4) containing various carbon sources (in mM: 5 glucose, 0.1 palmitate, 4 glutamine, 5 galactose, 5 lactate, 1 pyruvate) and either 10 mM 2-deoxyglucose or 20 µM etomixir as detailed in results. All conditions with palmitate had 0.1 mM L-carnitine. Oxygen consumption rates (OCR) were measured using an XF96 extracellular flux analyzer.

Ex-vivo Heart Perfusion

Mouse hearts were perfused in constant flow (4ml/min) Langendorff mode as previously described (3). Krebs-Henseleit buffer (KH, in mM: 118 NaCl, 4.7 KCl, 25 $NaHCO_3$, 1.2 $MgSO_4$, 1.2 KH_2PO_4, and 2.5 $CaCl_2$,

gassed with 95/5 O_2/CO_2, 37 °C) was supplemented with either 5 mM glucose, or 0.1 mM BSA-conjugated palmitate. Left ventricular pressure was measured via a water-filled transducer-linked left ventricular balloon. Left ventricular and coronary root pressures were monitored and digitally recorded at 1 kHz (DATAQ, Akron OH). After equilibration hearts were treated with isoproterenol (100 nM final) for 5 min.

Electron Microscopy

Hearts were fixed in 4 % paraformldehyde + 2.5 % glutaraldehyde in Millonig's phosphate buffer (0.2 M NaH_2PO_4/Na_2HPO_4, 0.5 % NaCl, pH 7.4). 1 mm cubes were processed and digitally photographed on a Hitachi 7650 electron microscope. Analysis of images was performed using NIH ImageJ software. Mitochondrial areas and density were placed in to 11 or 13 bins respectively and the resulting histograms were fitted to a single Gaussian. Form-factor was calculated as $1/((4 \rightarrow \text{area})/(\text{perimeter}^2))$ and aspect-ratio was calculated as (major axis/minor axis).

Metabolomics

WT and *Kcnt2*$^{-/-}$ hearts (N=7 per group) were perfused as above in KH buffer supplemented with glucose plus palmitate for 20 min., then freeze-clamped with Wollenberger tongs in liquid N_2 and ground to powder. Samples representing ~50% of each heart (50 mg) were shipped to Metabolon Inc. (Research Triangle Park, NC) on dry ice, extracted by standard procedures, and analyzed by LC-MS/MS and GC-MS/MS (Metabolon "Global Metabolomics" solution) to measure the relative steady-state abundance of metabolites.

Data for each run were median-normalized. Overall, 527 metabolites were identified, of which 26 (4.9%) were removed due to insufficient replicates, yielding 7014 theoretical individual data points (501 x N=7 x 2 groups). A further 229 outliers (>1 standard deviation from the mean) were removed, representing 3.3 % of the data. Missing values were imputed as weighted medians (26). Metabolomic data were analyzed using free Metaboanalyst software (27). In a separate series of experiments, WT and *Kcnt2*$^{-/-}$ hearts were perfused in KH buffer supplemented with fat as the only carbon source, and adenine nucleotide levels (ATP, ADP, AMP) were measured as previously described (28). Energy charge was calculated as (ATP+½ADP/(ATP+ADP+AMP).

Immunoblotting

Sample protein was determined by the Folin-Phenol (Lowry) assay. Non-mitochondrial samples were diluted 2x in Laemmli sample loading buffer (SLB) and incubated at 95 °C for 1 min., while mitochondrial samples were diluted 2x in SLB containing 5x the standard concentration of SDS and incubated at 25 °C for 30 min. Samples were separated by SDS-PAGE (10% gels) and transferred to nitrocellulose, followed by probing with antibodies as recommended by manufacturer protocols. Detection employed HRP-linked secondary

antibodies with enhanced chemiluimnescence (GE Biosciences). Developed ECL film images were quantified by densitometry using NIH ImageJ software (N=3-4 mice per genotype).

Body Composition, Fasting Glucose Response, and Electrocardiogram

84 day old (12 week) WT and littermate *Kcnt2*$^{-/-}$ male mice were anesthetized as described above, and body fat content measured using dual energy X-ray absorptometry (DEXA) scanning (Lunar PIXImus densitometer, GE, Fitchburg WI). Blood glucose was measured using a True2Go™ glucose meter with TrueTest™ glucose strips (Trividia Health, Fort Lauderdale FL). Mice were fasted overnight in cleaned cages with access to water and cotton bedding. Alternatively, after anesthesia mice electrocardiograms were recorded using a three electrode EKG amplifier (Harvard Apparatus, Cambridge MA). EKGs were averaged for each animal from ten different segments of the trace, each containing R_1-S_1-T_1-P_2-Q_2-R_2 waves.

qPCR analysis

mRNA was extracted from heart homogenates with acid phenol/TRIzol according to the Direct-zol RNA MiniPrep Kit R2050 (Zymo Research, Irvine CA) as described (29). cDNAs were prepared using an iScript kit (170-8891, BioRad). qPCR analysis was performed using a BioRad PrimePCR^{TM} "Regulation of lipid metabolism-PPAR" M96 Predesigned 96-well panel for use with SYBR® Green (Cat # 10031585).

Replicates & Statistics

Numbers of individual replicates for experiments are listed in each figure legend. For samples comparing WT and *Kcnt2*$^{-/-}$, one "N" equals one animal (i.e., biological replicates). Statistical differences between WT and *Kcnt2*$^{-/-}$ were determined using two-way ANOVA with a Bonferroni correction for multiple testing, followed by post-hoc paired or non-paired *t*-tests ($p<0.05$ cut-off).

Results

Kcnt2 knockout

Figure 1A shows the result of a genotyping experiment on WT and *Kcnt2*$^{-/-}$ mice, indicating the expected amplicons (see methods). The deletion targets exon 22 of the protein, and results in no residual protein in the knockouts (18), as we have also previously confirmed in the heart (3).

Cardiac Mitochondria Contain a $K_{Na}1.2$ Channel

To investigate cardiac mitochondrial K^+ channels, we performed electrophysiology studies on Percoll™-purified isolated mitochondrial inner membranes (mitoplasts) from hearts of wild type (WT) or *Kcnt2*$^{-/-}$ mice

(schematic, Figure 1C). Mitochondrial enrichment was verified by western blotting for mitochondrial proteins, and purity was confirmed by western blotting for non-mitochondrial membrane proteins (Figure 1D). Mitoplasts were readily identified under light microscopy (Figure 1C) and high resistance seals (2-10 G→) were formed with the inner membrane opposite the outer membrane cap. In a preliminary series of experiments using attached mitoplast patch configuration, channel activity in WT was not activated by NaCl alone, but manifested upon further addition of the K_{Na} activator bithionol (BT) (3). No activation by NaCl or BT was seen in *Kcnt2*$^{-/-}$ mitoplasts (Figure 1E/F). The absence of activation by NaCl alone in WT mitoplasts suggested that the channel's ion-sensing site may be on the matrix side of the inner membrane, and thus inaccessible to Na^+ from the bath perfusion on this time scale. To investigate such a channel, excised mitoplast patch was employed, affording access to the matrix side of the inner membrane (Figure 1C).

Channel activity was observed in a high proportion of independent preparations obtained from both WT (85%) and *Kcnt2*$^{-/-}$ (76%) hearts (Figure 2A), consistent with previous reports that mitochondria contain numerous K^+ channels (1, 30). A multiple level screen was performed to triage recordings containing channels other than K_{Na}1.2 (Figure 2B-D). The bath recording solution was sequentially switched from initial (containing 100 µM $CaCl_2$), to 40 mM LiCl, then 40 mM NaCl, and finally 40 mM NaCl plus 2.5 µM BT. Under each condition, channel activity was monitored at holding potentials from -100 mV to +100 mV.

First, patches exhibiting channel activity in Ca^{2+} alone were discarded, as this is indicative of K_{Ca} channel activity (Figure 2B, gold). Next, we discarded patches exhibiting activity following the switch to LiCl, as this is indicative of Na^+-conductance (31) (Figure 2B, light gray). Next, patches exhibiting channel activity in the presence of activating levels of NaCl (40mM) and NaCl plus BT (2.5 µM) were considered potential K_{Na}1.2 candidates (Figure 2C blue). Recordings exhibiting channel activity in the presence of Na^+ but not following BT addition, were also discarded (Figure 2C dark gray). Finally, single channel unitary conductance was compared to expected values for K_{Na}1.2 (~140 pS) (15, 31, 32) and those patches exhibiting appropriate conductance were considered to be K_{Na}1.2 channels worthy of further analysis (Figure 2D red).

Figure 2E shows representative recordings observed in mitoplast patches from WT and *Kcnt2*$^{-/-}$ mice, exhibiting a variety of unitary conductances, with the knockouts having an absence of activity in the conductance range expected for K_{Na}1.2. Quantitation of all conductances showed a cluster of 6 channels in WT mitoplasts that passed all screens (Figure 2F red data points), with no channels of similar conductance observed in *Kcnt2*$^{-/-}$ mitoplasts. The *Kcnt2*$^{-/-}$ recordings contained proportionally more Na^+ and BT activated channels than WT in the small conductance range (Figure 2F, black symbols in 20-80 pS range, *Kcnt2*$^{-/-}$ 6 of 42 vs. WT 2 of 25). A similar observation has been made for a mitochondrial BK channel, wherein loss of the expected conductance in a knockout was accompanied by appearance of smaller conductances (12). Figure 2G shows representative examples of single channel activity for three (of six) Na^+ and BT activated conductances

recorded at a holding potential of -40 mV in WT mitoplasts. As previously reported for $K_{Na}1.2$ (15), these channels showed rapid flickering between open and closed states. The average unitary slope conductance was 138±1 pS (Figure 2H: peak conductance graph for all six channels). Under our buffer conditions, reversal potential for channels conducting Na^+ or Cl^- is predicted to be -23 mV or -8 mV respectively. Since K^+ is the only other ion present, and the channel current crossed zero at -2 mV, this indicates that K^+ is the predominant conducting ion. Together, the data in Figure 2 demonstrate that WT cardiac mitochondria contain a K^+ channel with the ion-selectivity, ion-sensitivity, pharmacology and conductance properties of $K_{Na}1.2$, that is absent in mitochondria from *Kcnt2*$^{-/-}$ mice.

Electrophysiologic Characterization of Mitochondrial $K_{Na}1.2$

A detailed single channel analyses of all 6 assigned $K_{Na}1.2$ patches was not possible due to the presence of two or more identical channels within some patches (Figure 3A), suggesting that $K_{Na}1.2$ channels may cluster in their endogenous membranes. Such clustering has been previously reported for $K_{Na}1.1$ channels in neuronal plasma-membranes (33). Examination of all suitable WT recordings (representative example Figure 3B) revealed a higher open probability at negative potentials (Figure 3C). In addition, as previously reported for $K_{Na}1.2$ (15, 35), numerous distinct subconductances were apparent between 35 and 140pS (Figure 3D). This behavior is characteristic of $K_{Na}1.1$ channels (*Kcnt1*/Slack/SLO2.2) (34, 35) and while it has been observed in $K_{Na}1.2$ mutants (36), this is the first observation of such in WT $K_{Na}1.2$ channels in endogenous membranes. The average slope conductance when considering all subconductances was 75 pS (Figure 3E), which agreed well with the average chord conductance of 74.8±6.8 pS (assuming reversal potential = 0 mV). These data indicate that smaller subconductance states predominate in the active channel current.

Open and closed channel dwell times were also calculated from continuous recordings at -40mV (representative 45 s. example, Figure 3F). The frequency of channel open and closed dwell times was fitted to the sum of multiple simple exponentials, constituting 94.6% of the total area under the curve, and subsequent log-binned histograms revealed peaks representing two open times and three closed times (Figure 3G). The longest closed time (τ_3 = 262 ms.) represents long periods of channel closure between bursts of activity, which is characteristic for $K_{Na}1.2$ (REF).

$K_{Na}1.2$ Channel Activation Uncouples Cardiomyocyte Oxidative Phosphorylation

We next sought to determine the impact of cardiac $K_{Na}1.2$ channel activity on cardiomyocyte bioenergetics. Using Seahorse™ extracellular flux (XF) analysis, we measured oxygen consumption rates (OCR) of cardiomyocytes from WT and *Kcnt2*$^{-/-}$ mice. Cells from both genotypes had similar viability and rod-shaped morphology (Figure 4A). Figure 4B shows that the K_{Na} opener BT (2.5 μM) significantly stimulated

OCR in oligomycin-treated cardiomyocytes from WT mice but not those from *Kcnt2*$^{-/-}$ mice (WT: 370±48 Max OCR; *Kcnt2*$^{-/-}$ 154±32 Max OCR). The small effect of BT seen in *Kcnt2*$^{-/-}$ cells is consistent with the observation of the small conductances activated by Na^+ and BT in *Kcnt2*$^{-/-}$ mitoplast patches (Figure 2F).

In the mitochondrial K^+ cycle (37), K^+ entry to the organelle activates a mitochondrial K^+/H^+ exchanger, such that mitochondrial K^+ channel activity can uncouple oxidative phosphorylation. As such, the much larger BT induced respiratory stimulation in WT vs. *Kcnt2*$^{-/-}$ cardiomyocytes is likely due to mitochondrial uncoupling. As an additional control, the bona-fide mitochondrial uncoupler FCCP elicited similar maximal respiration rates in cardiomyocytes from both genotypes WT: 387±15 Max OCR; *Kcnt2*$^{-/-}$ 364.2±53 Max OCR), rendering it unlikely that the differential effect of BT in WT vs. *Kcnt2*$^{-/-}$ cells was due to an underlying difference in overall bioenergetic capacity. Consistent with this, western blotting for a number of mitochondrial marker enzymes (SDHA, ICDH, Cyp-D, and ETFA) suggested no difference in mitochondrial mass or content between WT and *Kcnt2*$^{-/-}$ hearts (Figure 4C).

Loss of K_{Na}1.2 Mildly Impacts Cardiac Mitochondrial Ultrastructure

An important function of the mitochondrial K^+ cycle is the regulation of organelle volume (38, 39), and K_{Na}1.2 activity is known to be sensitive to osmolarity (40, 41). Thus we hypothesized that mitochondria from *Kcnt2*$^{-/-}$ may exhibit ultrastructural changes. Electron-microscopic analysis of hearts from WT and *Kcnt2*$^{-/-}$ mice (Figure 4D-F) revealed that mitochondria had similar area (WT: 0.51±0.30 μm^2, *Kcnt2*$^{-/-}$: 0.53±0.32 μm^2, means±SD, N=3-4) and matrix density (WT: 109±13, *Kcnt2*$^{-/-}$: 102±11, means±SD, N=3-4). However, the distribution of these parameters (Figure 4E) suggests a small shift toward increased area and density in *Kcnt2*$^{-/-}$ vs. WT. Additionally, no difference in either form-factor or aspect-ratio was observed between genotypes (Figure 4F), indicating that K_{Na}1.2 deficiency does not alter mitochondrial fission or fusion (42, 43). Together, the data in Figure 4 suggest that although activation of K_{Na}1.2 can uncouple respiration, loss of the channel does not impact cardiac mitochondrial structure or content.

K_{Na}1.2 is Required for Cardiac Respiratory Reserve Capacity when Oxidizing Fat

In an effort to further understand the bioenergetic effects of K_{Na}1.2 deficiency we compared metabolic substrate preferences in cardiomyocytes isolated from WT and *Kcnt2*$^{-/-}$ mice. Myocytes were incubated with either: (i) glucose alone (with etomoxir to inhibit fatty acid →oxidation), (ii) palmitate alone (with 2-deoxyglucose to inhibit glycolysis), or (iii) glucose plus palmitate. The response to uncoupling by FCCP (500 nM) was used to determine "respiratory reserve" (RR) capacity under each substrate condition (Figures 5A-C).

Cardiomyocytes from WT and *Kcnt2*$^{-/-}$ cells exhibited a similar baseline OCR under all substrate conditions (Figure 5B open bars). In WT cells, a robust uncoupling response to FCCP was seen under all

conditions, and notably the uncoupling response with palmitate alone (3.3 fold) was equal to that seen when both substrates were present (3.3 fold). However, in *Kcnt2*$^{-/-}$ cells, the uncoupling response with palmitate alone (2.4 fold) was significantly blunted compared to that seen when both substrates were present (4.3 fold) (comparison between blue and purple bars in left & right panels of Figure 5B). The additional OCR induced over baseline by FCCP is used to calculate RR capacity. Figure 5C shows that the RR of WT and *Kcnt2*$^{-/-}$ cells is similar in either the glucose alone or the glucose plus palmitate conditions (red and purple bars respectively). However, with palmitate alone (blue bars), *Kcnt2*$^{-/-}$ cells exhibit a significant RR deficit relative to WT. Notably, no such RR deficit was observed in myocytes from *Kcnt2*$^{-/-}$ mice respiring on lactate, glutamine, galactose, or pyruvate (Figure 5D), indicating the *Kcnt2*$^{-/-}$ RR deficit is specific to fat oxidation.

To test the physiologic relevance of this RR deficit, the ability of perfused hearts to respond to increased metabolic demand was tested. Hearts from WT and *Kcnt2*$^{-/-}$ mice were perfused with palmitate as the sole carbon source, while stimulating workload by addition of the →adrenergic agonist isoproterenol (100nM). Hearts from *Kcnt2*$^{-/-}$ mice showed a significantly reduced functional response to isoproterenol, relative to WT (WT: 213±20 % vs. *Kcnt2*$^{-/-}$: 159±13 %, means±SEM, N=7) (Figure 6A). However, consistent with the isolated cardiomyocyte OCR data (Figure 5C), no difference in the isoproterenol-induced functional response was observed when the perfusion buffer was supplemented with glucose and palmitate (Figure 6A). Together, these data suggest that loss of $K_{Na}1.2$ results in an impaired ability to respond to increased metabolic demand when oxidizing only fat. Consistent with previous reports (3, 18) no EKG differences were observed in *Kcnt2*$^{-/-}$mice (Figure 6B), suggesting that loss of $K_{Na}1.2$ *per se* does not impact cardiac contractile function.

Whole Animal Metabolic Differences in Kcnt2$^{-/-}$ *Mice*

Since the heart is an major fat-burning organ, we hypothesized that the fat-specific RR capacity deficit in *Kcnt2*$^{-/-}$ might be accompanied by metabolic perturbations at the whole animal level. No significant differences in weight gain were observed between WT and *Kcnt2*$^{-/-}$ mice over 25 weeks (Figure 7A). Analysis of percent body fat content by differential energy X-ray absorptometry analysis (DEXA, Figure 7B) revealed a small difference in average fat content between genotypes (WT: 12.1±2.8 % vs. *Kcnt2*$^{-/-}$: 13.6±3.3 %), but nevertheless this difference was statistically significant between paired littermates (Figure 7C). In addition, while WT mice showed an expected drop in blood glucose following an overnight (15 hr.) fast, no such drop was seen in *Kcnt2*$^{-/-}$ mice (Figure 7D). This suggests elevated gluconeogenesis in response to fasting in *Kcnt2*$^{-/-}$, which is consistent with a potential increased reliance on glucose oxidation as a compensatory response to the fat-specific RR defect under stress conditions.

Metabolomic and Expression Profiling of Kcnt2$^{-/-}$ *Hearts*

To investigate the molecular underpinnings of the fat-specific RR defect in *Kcnt2*$^{-/-}$ hearts, expression of metabolic regulatory genes was measured using a predesigned qPCR array (Figure 8A, Table 1). No differences were observed between WT and *Kcnt2*$^{-/-}$ hearts, suggesting the fat-specific RR defect is not due to a remodeling of metabolism at the gene level. Separately, a small but non-significant decrease in energy charge (ATP+½ADP/(ATP+ADP+AMP)) was observed in *Kcnt2*$^{-/-}$ mice (WT: 0.87±0.05 vs. *Kcnt2*$^{-/-}$: 0.77±0.03, mean±SEM, N=5-6), suggesting that energy-sensing metabolic regulators such as AMP dependent protein kinase (AMPK) may be altered. However, western blotting analysis revealed no difference in AMPK phosphorylation between WT and *Kcnt2*$^{-/-}$ hearts (data not shown). Together with data in Figures 4 and 5, these findings suggest that K_{Na}1.2 deficiency does not induce large scale remodeling of cardiac mitochondrial metabolism. Rather, K_{Na}1.2 loss specifically impacts cardiac fat oxidation, only under conditions of high energy demand such as uncoupling or →adrenergic stimulation.

Finally, to understand the effects of K_{Na}1.2 deficiency on cardiac metabolism at a systems level, an unbiased metabolomics analysis was performed. Principal component analysis (PCA) showed no significant difference in the fundamental character of metabolism between WT and *Kcnt2*$^{-/-}$hearts at baseline (Figure 8B). A volcano plot for all 501 metabolites measured revealed only 10 were significantly altered (>1.5-fold vs. WT, $p<0.05$) (Figure 8C). Of these metabolites, notable changes were an increase in phenol-sulfate and decrease in dimethyl-sulfone, potentially indicating perturbations in aryl-sulfotransferase activity and sulfur metabolism. Dehydroascorbate was significantly lower in *Kcnt2*$^{-/-}$ hearts, potentially indicating lower oxidative load. In addition, inositol-1-phosphate was significantly elevated, and a cluster of diacylglycerol metabolites was also elevated (although no individual DAG approached significance), suggesting enhanced phospholipase C activity in *Kcnt2*$^{-/-}$. Overall, the comparatively minor nature of metabolomic perturbations in *Kcnt2*$^{-/-}$ hearts at baseline is consistent with the notion that the impact of K_{Na}1.2 loss is limited to fat oxidation under conditions of high energy demand.

Discussion

A plethora of studies has identified mitochondrial K^+ channels at the phenomenological level (reviewed in (1, 44)), and several studies have linked these channels mechanistically to protection against IR injury (1, 45–47). However, surprisingly few examples exist of bona-fide mitochondrial K^+ channels that are: (i) identified at the molecular (genetic) level, (ii) characterized with robust electrophysiology, and (iii) linked to any specific mitochondrial channel function phenotype (examples include K_{Ca}1.1 (11, 12), K_{ATP} (10), and SK3 (48)). While the phenomenon of a K_{Na} channel was first characterized in hearts thirty years ago, the field of K_{Na} research rapidly transitioned to study of these channels in brain (19). As such, very little is known about role of K_{Na} in cardiomyocytes, including sub-cellular localization. Using patch-clamp studies of isolated cardiac

mitochondrial inner membranes, we recorded a K^+ channel matching the known characteristics of $K_{Na}1.2$ (ion-sensitivity, ion-selectivity, pharmacology and conductance) in mitoplasts from WT mice, that was absent in those from *Kcnt2*$^{-/-}$ mice (Figures 1-3). This is the first report of a K_{Na} channel in mitochondria.

Since cardiac mitochondria are reported to contain several cation and anion channels (49, 50), mitoplast recordings were subjected to a rigorous screening process to ensure that conductances assigned as $K_{Na}1.2$ did not originate from other channels. Bath/pipette ratios of the major ion components (K^+, Na^+, and Cl^-) enabled reversal potentials to be differentiated. The Na^+ surrogate Li^+ was used to screen out any Na^+-activated currents that were in fact due to Na^+ conductance. In addition, any conductances activated by Ca^{2+} were dismissed, to ensure patched membranes were free of K_{Ca} channels. Anion channels of the IMAC and CLIC variety exhibit conductances (~100pS: IMAC, ~8pS: CLIC4) sufficiently distinct from $K_{Na}1.2$ that, in combination with the observed reversal potential, we are confident do not contribute to assigned K_{Na} conductances. Similarly mitoK_{ATP} channels (~10pS) would not be mistaken for $K_{Na}1.2$. Finally, $K_{Na}1.2$ activation is significantly enhanced by Cl^- in the presence of activating Na^+, hence Cl^- salts were used to maximize the probability of detecting these channels (15). Of 25 recordings in WT mitoplasts, this strategy yielded 6 channels, a 24% success rate. Application of this rate to the 42 recordings in *Kcnt2*$^{-/-}$ mitoplasts predicts 10 such channels, but we observed zero.

Several known electrophysiologic characteristics of $K_{Na}1.2$ channels were also observed in our assigned $K_{Na}1.2$ mitoplast recordings, including: (i) multiple sub-conductance states (Figure 3D) (15, 36), (ii) rapid flickering between open and closed states (Figure 2G) (15), (iii) burst operation with prolonged closed times between bursts (Figure 3F/G) (15, 51), and (iv) multiple channels within the same patch suggesting channel clustering in membranes (Figure 3A) (36). In combination with the absence of such conductances in *Kcnt2*$^{-/-}$ mitoplasts, these characteristics strengthen the conclusion that the genetic origin of the channels herein assigned as mito-$K_{Na}1.2$, is the *Kcnt2* gene product. Whole mitoplast attached patch experiments (Figure 1E) suggest that the orientation of the channel in the mitochondrial inner membrane is the same as that reported for plasma membrane $K_{Na}1.2$, namely with the c-terminal Na^+ sensing site on the inside of the membrane (15, 52).

Patches from WT and *Kcnt2*$^{-/-}$ recordings contained channels with a similar overall range of conductances. However, the distribution of these conductances between genotypes was shifted. In particular, channels with unitary conductances in the range of 20-80pS were more frequently observed in *Kcnt2*$^{-/-}$ (Figure 2F). A similar observation was recently made using a cardiac-specific knockout of the mito-BK channel (12), raising the intriguing possibility that loss of one mitochondrial K^+ channel may lead to compensatory up-regulation of other channels, to maintain K^+ homeostasis. Given the importance of the mitochondrial K^+ cycle for the regulation of organelle volume (37), such compensatory K^+ fluxes may account for the persistence of a small but non-significant respiratory uncoupling effect of BT in *Kcnt2*$^{-/-}$ cardiomyocytes (Figure 4B), as well as

the relatively minor effect of $K_{Na}1.2$ loss on mitochondrial ultrastructure (Figure 4D-F). An alternative to compensatory expression between different mitochondrial K^+ channels, is the possibility they may form heteromers. Indeed, individual $K_{Na}1.1$ (*Kcnt1*) subunits can combine with $K_{Ca}1.1$ (*Kcnma1*) subunits to form functional heterotetramers of intermediate conductance and activation properties (14). Heterotetramers of $K_{Na}1.1$ with $K_{Na}1.2$ have also been demonstrated (36). However, the existence of $K_{Ca}1.1/K_{Na}1.2$ heterotetramers has not been reported.

A key aspect of these studies was the discovery that loss of cardiac $K_{Na}1.2$ results in a unique metabolic phenotype, namely a specific defect in cardiac fat oxidation only under conditions of high energy demand. An important caveat is that we cannot currently rule out the possibility that the metabolic phenotype of *Kcnt2*$^{-/-}$ is due to loss of the channel at the plasma membrane. However, evidence for the existence of K_{Na} channels at the cardiac plasma membrane comprises a single study 30 years ago (19). Despite the development of anti-K_{Na} antibodies, fluorescent tags, and K_{Na} channel knockout animals, confirmation of the channel's existence at the cardiac plasma membrane has not been confirmed using any of these methods during the intervening time period. Coupled with definitive data herein demonstrating existence of $K_{Na}1.2$ in mitochondria, and previous reports of a BT activated mitochondrial K^+ channel that is absent in mitochondria isolated from *Kcnt2*$^{-/-}$, we assert that the most likely explanation for a mitochondrial/metabolic phenotype in *Kcnt2*$^{-/-}$, is loss of the channel in mitochondria.

The metabolic phenotype of *Kcnt2*$^{-/-}$ (Figures 5-6) was manifest under conditions corresponding to classical bioenergetic "state 3", wherein the mitochondrial membrane potential is consumed to generate ATP. As such, if the *in-situ* reversal potential of mitochondrial $K_{Na}1.2$ is above zero, then channel opening could readily occur under conditions of high energetic demand when potential is lowered. In addition, the mitochondrial membrane potential is known to "flicker" *in-vivo* (53), such that transient depolarization events may activate mito-$K_{Na}1.2$. These properties may render mitochondrial $K_{Na}1.2$ function important under conditions of stress, such as tissue ischemia. Given the previously reported requirement of $K_{Na}1.2$ for cardioprotection by APC (3), it is notable that the mitochondrial membrane potential depolarizes and cytosolic Na^+ levels also rise during ischemia (54, 55). Together, these observations suggest that mito-$K_{Na}1.2$ channels may be activated by acute perturbations in mitochondrial energy demand or under stress conditions such as ischemia. Such properties may explain why the metabolic phenotype of *Kcnt2*$^{-/-}$ is only evident under stress.

The data in Figure 7 revealed additional chronic effects of $K_{Na}1.2$ loss on bioenergetics that resulted in altered body fat content and fasting glucose metabolism. Due to the presence of a mitochondrial K^+/H^+ exchanger (KHE), activation of a mitochondrial K^+ channel would be expected to decrease the mitochondrial –pH, thus uncoupling oxidative phosphorylation and stimulating OCR, as shown in Figure 4B. As such, mild mitochondrial uncoupling by mito-$K_{Na}1.2$ channel activators may represent a novel therapeutic avenue for

obesity/diabetes/metabolic-syndrome. It is therefore notable that the anti-helminthic drug niclosamide, which activates K_{Na} channels (56), has long been known to uncouple mitochondria (57), and was recently shown to confer benefits in a mouse high-fat diet model of diabetes (58). Furthermore, a recent case report highlighted a patient with a $K_{Na}1.2$ mutation ($Q_{270}E$) suffering from migrating focal seizures that were non-responsive to the ketogenic diet typically used to treat such symptoms (59). Cardiac metabolomics also revealed a potential up-regulation of phospholipase C (PLC) signaling in the *Kcnt2*$^{-/-}$ heart (Figure 8C). Since $K_{Na}1.2$ channels are known to interact with the PLC substrate PIP_2 (60), this raises the possibility that loss of $K_{Na}1.2$ results in perturbation of PIP_2/PLC signaling. An important PLC downstream target is protein kinase C epsilon (PKCε), which is known to play a role in development of insulin resistance in response to a high fat diet (61). As such, in addition to mitochondrial uncoupling, mito-$K_{Na}1.2$ channel activators may confer metabolic benefits via a PIP_2/PLC/PKCε signaling axis. A deeper investigation of the relationship between mito-$K_{Na}1.2$ activity and metabolic regulation is thus warranted.

Disclosures

None

Acknowledgments.

We thank Christopher Lingle (Washington University, St Louis MO) for providing founders for the *Kcnt2*$^{-/-}$ mice, and Kathleen Kinally (New York University, Emeritus) for technical support in performing mitochondrial patch clamp experiments. We also thank Dana Godfrey (URMC musculoskeletal center) for support with DEXA analyses, and Karen Bentley (URMC electron microscopy core).

Author Contributions

Charles O. Smith, Paul S. Brookes, and Keith Nehrke designed research. Charles O. Smith, Yves T. Wang, Sergiy M. Nadtochiy, and James H. Miller performed experiments. Yves T. Wang developed software for analysis of Langendorff traces. Charles O. Smith analyzed data. Charles O. Smith, and Paul S. Brookes wrote paper. Elizabeth A. Jonas, and Robert T. Dirksen contributed new analytical tools, training, and critical resources. This work was funded by grants from the National Institutes of Health: R01-GM087483 (to Paul S. Brookes, and Keith Nehrke), R01-HL071158 (to Paul S. Brookes) and R01-AR-059646 (to Robert, T. Dirksen).

References

1. Smith, C. O., Nehrke, K., and Brookes, P. S. (2017) The Slo(w) path to identifying the mitochondrial channels responsible for ischemic protection. *Biochem. J.* **474**, 2067–2094
2. Bentzen, B. H., Nardi, A., Calloe, K., Madsen, L. S., Olesen, S.-P., and Grunnet, M. (2007) The Small Molecule NS11021 Is a Potent and Specific Activator of Ca2+-Activated Big-Conductance K+ Channels. *Mol. Pharmacol.* **72**, 1033–1044
3. Wojtovich, A. P., Smith, C. O., Urciuoli, W. R., Wang, Y. T., Xia, X.-M., Brookes, P. S., and Nehrke, K. (2016) Cardiac Slo2.1 Is Required for Volatile Anesthetic Stimulation of K+ Transport and Anesthetic Preconditioning. *Anesthesiology* **124**, 1065–1076
4. Garlid, K. D., Paucek, P., Yarov-Yarovoy, V., Murray, H. N., Darbenzio, R. B., D'Alonzo, A. J., Lodge, N. J., Smith, M. A., and Grover, G. J. (1997) Cardioprotective effect of diazoxide and its interaction with mitochondrial ATP-sensitive K+ channels. Possible mechanism of cardioprotection. *Circ. Res.* **81**, 1072–1082
5. Inoue, I., Nagase, H., Kishi, K., and Higuti, T. (1991) ATP-sensitive K+ channel in the mitochondrial inner membrane. *Nature* **352**, 244–247
6. Dolga, A. M., Netter, M. F., Perocchi, F., Doti, N., Meissner, L., Tobaben, S., Grohm, J., Zischka, H., Plesnila, N., Decher, N., and Culmsee, C. (2013) Mitochondrial small conductance SK2 channels prevent glutamate-induced oxytosis and mitochondrial dysfunction. *J. Biol. Chem.* **288**, 10792–10804
7. Nabbi, R., Gadicherla, A. K., Kersten, J. R., Stowe, D. F., Lazar, J., and Riess, M. L. (2014) Genetically determined mitochondrial preservation and cardioprotection against myocardial ischemia-reperfusion injury in a consomic rat model. *Physiol. Genomics* **46**, 169–176
8. Siemen, D., Loupatatzis, C., Borecky, J., Gulbins, E., and Lang, F. (1999) Ca2+-activated K channel of the BK-type in the inner mitochondrial membrane of a human glioma cell line. *Biochem. Biophys. Res. Commun.* **257**, 549–554
9. Singh, H., Lu, R., Bopassa, J. C., Meredith, A. L., Stefani, E., and Toro, L. (2013) MitoBK(Ca) is encoded by the Kcnma1 gene, and a splicing sequence defines its mitochondrial location. *Proc. Natl. Acad. Sci. U. S. A.* **110**, 10836–10841
10. Foster, D. B., Ho, A. S., Rucker, J., Garlid, A. O., Chen, L., Sidor, A., Garlid, K. D., and O'Rourke, B. (2012) Mitochondrial ROMK channel is a molecular component of mitoK(ATP). *Circ. Res.* **111**, 446–454
11. Soltysinska, E., Bentzen, B. H., Barthmes, M., Hattel, H., Thrush, A. B., Harpeu/#P l-H#H1/#Tyr uwxs /#N1/#

Oduvhq/#I 1#M#Vfkl iihu/#W#D1/#Or vd-Uh| qd/#M#Vwdxe lqj hu/#M#Nql hvv/#D1/#Wkr p vhq/#P 1#E 1#E1/#
Eu¨ j j hp dqq/#D1/#I hqvnh/#V1/#Elho/#P 1/#Uxvk/#S1/#Z dko-Vfk ww#F 1/#Er xvkho/#U1#F 1/#R dvhq/#V1-S1#S1/#
Oxnr z vnl/#U1/#

Yan, Y., Sigworth, F. J., and Kaczmarek, L. K. (2006) Pharmacological activation and inhibition of Slack (Slo2.2) channels. *Neuropharmacology* **51**, 896–906

21. Szabo, I. and Zoratti, M. (2014) Mitochondrial channels: ion fluxes and more. *Physiol. Rev.* **94**, 519–608
22. Murphy, E. and Eisner, D. A. (2009) Regulation of Intracellular and Mitochondrial Sodium in Health and Disease. *Circ. Res.* **104**, 292–303
23. Nita, I. I., Hershfinkel, M., Lewis, E. C., and Sekler, I. (2015) A crosstalk between Na+ channels, Na+/K+ pump and mitochondrial Na+ transporters controls glucose-dependent cytosolic and mitochondrial Na+ signals. *Cell Calcium* **57**, 69–75
24. Bay, J., Kohlhaas, M., and Maack, C. (2013) Intracellular Na+ and cardiac metabolism. *J. Mol. Cell. Cardiol.* **61**, 20–27
25. Murphy, E. and Eisner, D. A. (2009) Regulation of Intracellular and Mitochondrial Sodium in Health and Disease. *Circ. Res.* **104**, 292–303
26. Aittokallio, T. (2010) Dealing with missing values in large-scale studies: microarray data imputation and beyond. *Brief. Bioinform.* **11**, 253–264
27. Xia, J. and Wishart, D. S. (2016) Using MetaboAnalyst 3.0 for Comprehensive Metabolomics Data Analysis. In *Current Protocols in Bioinformatics* vol. 55, p. 14.10.1-14.10.91, John Wiley & Sons, Inc., Hoboken, NJ, USA
28. Nadtochiy, S. M., Urciuoli, W., Zhang, J., Schafer, X., Munger, J., and Brookes, P. S. (2015) Metabolomic profiling of the heart during acute ischemic preconditioning reveals a role for SIRT1 in rapid cardioprotective metabolic adaptation. *J. Mol. Cell. Cardiol.* **88**, 64–72
29. Toledo-Arana, A., Dussurget, O., Nikitas, G., Sesto, N., Guet-Revillet, H., Balestrino, D., Loh, E., Gripenland, J., Tiensuu, T., Vaitkevicius, K., Barthelemy, M., Vergassola, M., Nahori, M.-A., Soubigou, G., Régnault, B., Coppée, J.-Y., Lecuit, M., Johansson, J., and Cossart, P. (2009) The Listeria transcriptional landscape from saprophytism to virulence. *Nature* **459**, 950–956
30. Szewczyk, A., Jarmuszkiewicz, W., and Kunz, W. S. (2009) Mitochondrial potassium channels. *IUBMB Life* **61**, 134–143
31. Dryer, S. E., Fujii, J. T., and Martin, A. R. (1989) A Na+-activated K+ current in cultured brain stem neurones from chicks. *J. Physiol.* **410**, 283–296
32. Kaczmarek, L. K. (2013) Slack, Slick and Sodium-Activated Potassium Channels. *ISRN Neurosci.* **2013**, 1–14
33. Kim, G. E., Kronengold, J., Barcia, G., Quraishi, I. H., Martin, H. C., Blair, E., Taylor, J. C., Dulac, O., Colleaux, L., Nabbout, R., and Kaczmarek, L. K. (2014) Human Slack Potassium Channel Mutations Increase Positive Cooperativity between Individual Channels. *Cell Rep.* **9**, 1661–1672

34. Kaczmarek, L. K., Aldrich, R. W., Chandy, K. G., Grissmer, S., Wei, A. D., and Wulff, H. (2017) International Union of Basic and Clinical Pharmacology . C . Nomenclature and Properties of Calcium-Activated and Sodium-Activated Potassium Channels. *Pharmacol. Rev.* **69**, 1–11

35. Kim, G. E. and Kaczmarek, L. K. (2014) Emerging role of the KCNT1 Slack channel in intellectual disability. *Front. Cell. Neurosci.* **8**, 209

36. Chen, H., Kronengold, J., Yan, Y., Gazula, V.-R. V.-R., Brown, M. R., Ma, L., Ferreira, G., Yang, Y., Bhattacharjee, A., Sigworth, F. J., Salkoff, L., and Kaczmarek, L. K. (2009) The N-terminal domain of Slack determines the formation and trafficking of Slick/Slack heteromeric sodium-activated potassium channels. *J. Neurosci.* **29**, 5654–5665

37. Garlid, K. D. (1996) Cation transport in mitochondria--the potassium cycle. *Biochim. Biophys. Acta* **1275**, 123–126

38. Bednarczyk, P., Wieckowski, M. R., Broszkiewicz, M., Skowronek, K., Siemen, D., and Szewczyk, A. (2013) Putative Structural and Functional Coupling of the Mitochondrial BKCa Channel to the Respiratory Chain. *PLoS One* **8**, e68125

39. Checchetto, V., Teardo, E., Carraretto, L., Leanza, L., and Szabo, I. (2016) Physiology of intracellular potassium channels: A unifying role as mediators of counterion fluxes? **1857**

40. Tejada, M. A., Hashem, N., Calloe, K., and Klaerke, D. A. (2017) Heteromeric Slick/Slack K+ channels show graded sensitivity to cell volume changes. *PLoS One* **12**, e0169914

41. Tejada, M. A., Stople, K., Hammami Bomholtz, S., Meinild, A.-K., Poulsen, A. N., and Klaerke, D. A. (2014) Cell volume changes regulate slick (Slo2.1), but not slack (Slo2.2) K+ channels. *PLoS One* **9**, e110833

42. Picard, M., White, K., and Turnbull, D. M. (2013) Mitochondrial morphology, topology, and membrane interactions in skeletal muscle: a quantitative three-dimensional electron microscopy study. *J. Appl. Physiol.* **114**, 161–171

43. Bugger, H., Dong, C., Riehle, C., Soto, J., Theobald, H. A., Hu, X., Ganesan, B., Weimer, B. C., and Abel, E. D. (2009) Tissue-specific remodeling of the mitochondrial proteome in type 1 diabetic akita mice. *Diabetes* **58**, 1986–1997

44. Laskowski, M., Augustynek, B., Kulawiak, B., Koprowski, P., Bednarczyk, P., Jarmuszkiewicz, W., and Szewczyk, A. (2016) What do we not know about mitochondrial potassium channels? *Biochim. Biophys. Acta - Bioenerg.* **1857**, 1247–1257

45. Testai, L., Rapposelli, S., Martelli, A., Breschi, M. C. C., and Calderone, V. (2015) Mitochondrial Potassium Channels as Pharmacological Target for Cardioprotective Drugs. *Med. Res. Rev.* **35**, 520–553

46. Ertracht, O., Malka, A., Atar, S., and Binah, O. (2014) The mitochondria as a target for cardioprotection

in acute myocardial ischemia. *Pharmacol. Ther.* **142**, 33–40

47. Tano, J.-Y. J.-Y. J.-Y. and Gollasch, M. (2014) Hypoxia and ischemia-reperfusion: a BiK contribution? *AJP Hear. Circ. Physiol.* **307**, H811–H817
48. Stowe, D. F., Gadicherla, A. K., Zhou, Y., Aldakkak, M., Cheng, Q., Kwok, W.-M., Jiang, M. T., Heisner, J. S., Yang, M., and Camara, A. K. S. S. (2013) Protection against cardiac injury by small Ca(2+)-sensitive K(+) channels identified in guinea pig cardiac inner mitochondrial membrane. *Biochim. Biophys. Acta* **1828**, 427–442
49. Ponnalagu, D. and Singh, H. (2016) Anion Channels of Mitochondria. In *Handbook of experimental pharmacology* vol. 240, pp. 71–101,
50. Leanza, L., Biasutto, L., Managò, A., Gulbins, E., Zoratti, M., and Szabò, I. (2013) Intracellular ion channels and cancer. *Front. Physiol.* **4**, 227
51. Yang, B., Desai, R., and Kaczmarek, L. K. (2007) Slack and Slick K(Na) channels regulate the accuracy of timing of auditory neurons. *J. Neurosci.* **27**, 2617–2627
52. Thomson, S. J., Hansen, A., and Sanguinetti, M. C. (2015) Identification of the intracellular Na^+ sensor in Slo2.1 potassium channels. *J. Biol. Chem.* **290**, 14528–14535
53. O'Reilly, C. M., Fogarty, K. E., Drummond, R. M., Tuft, R. A., Walsh, J. V, and Jr. (2003) Quantitative analysis of spontaneous mitochondrial depolarizations. *Biophys. J.* **85**, 3350–3357
54. Green, D. R. and Kroemer, G. (2004) The pathophysiology of mitochondrial cell death. *Science* **305**, 626–629
55. Lesnefsky, E. J., Moghaddas, S., Tandler, B., Kerner, J., and Hoppel, C. L. (2001) Mitochondrial Dysfunction in Cardiac Disease: Ischemia–Reperfusion, Aging, and Heart Failure. *J. Mol. Cell. Cardiol.* **33**, 1065–1089
56. Biton, B., Sethuramanujam, S., Picchione, K. E., Bhattacharjee, A., Khessibi, N., Chesney, F., Lanneau, C., Curet, O., and Avenet, P. (2012) The antipsychotic drug loxapine is an opener of the sodium-activated potassium channel slack (Slo2.2). **340**
57. Weinbach, E. C. and Garbus, J. (1969) Mechanism of action of reagents that uncouple oxidative phosphorylation. *Nature* **221**, 1016–1018
58. Tao, H., Zhang, Y., Zeng, X., Shulman, G. I., and Jin, S. (2014) Niclosamide ethanolamine–induced mild mitochondrial uncoupling improves diabetic symptoms in mice. *Nat. Med.* **20**, 1263–1269
59. Madaan, P., Jauhari, P., Gupta, A., Chakrabarty, B., and Gulati, S. (2017) A quinidine non responsive novel KCNT1 mutation in an Indian infant with epilepsy of infancy with migrating focal seizures. *Brain Dev.*
60. Tejada, M. de los A., Jensen, L. J., and Klaerke, D. A. (2012) PIP2 modulation of Slick and Slack K+

channels. *Biochem. Biophys. Res. Commun.* **424**, 208–213

61. Samuel, V. T., Liu, Z.-X., Wang, A., Beddow, S. A., Geisler, J. G., Kahn, M., Zhang, X., Monia, B. P., Bhanot, S., and Shulman, G. I. (2007) Inhibition of protein kinase Cepsilon prevents hepatic insulin resistance in nonalcoholic fatty liver disease. *J. Clin. Invest.* **117**, 739–745

Table 1. Gene names and symbols for genes targeted by BioRad PrimePCR qPCR assay kit (Figure 8A)

Gene Name	Gene Symbol
Acetyl-Coenzyme A acyltransferase 1A	Acaa1a
Carnitine palmitoyltransferase 1a, liver	Cpt1a
Hydroxyacyl-Coenzyme A dehydrogenase/3-ketoacyl-Coenzyme A thiolase/enoyl-Coenzyme A hydratase (trifunctional protein), alpha subunit	Hadha
Acyl-Coenzyme A dehydrogenase, medium chain	Acadm
Carnitine palmitoyltransferase 1b, muscle	Cpt1b
Hydroxyacyl-Coenzyme A dehydrogenase/3-ketoacyl-Coenzyme A thiolase/enoyl-Coenzyme A hydratase (trifunctional protein), beta subunit	Hadhb
Glyceraldehyde-3-phosphate dehydrogenase	Gapdh
Acyl-Coenzyme A oxidase 3, pristanoyl	Acox3
Carnitine palmitoyltransferase 2	Cpt2
Hypoxanthine guanine phosphoribosyl transferase	Hprt
Acyl-CoA synthetase long-chain family member 1	Acsl1
Enoyl-Coenzyme A, hydratase/3-hydroxyacyl Coenzyme A dehydrogenase	Ehhadh
Retinoid X receptor alpha	Rxra
PrimePCR DNA Contamination Control Assay	gDNA
Fatty acid binding protein 1, liver	Fabp1
Solute carrier family 25 (mitochondrial carnitine/acylcarnitine translocase), member 20	Slc25a20
PrimePCR Positive Control Assay	PCR
Acyl-CoA synthetase long-chain family member 4	Acsl4
Solute carrier family 27 (fatty acid transporter), member 1	Slc27a1
PrimePCR RNA Quality Assay	RQ1
Fatty acid binding protein 3, muscle and heart	Fabp3
CD36 antigen	Cd36
Fatty acid binding protein 4, adipocyte	Fabp4
Uncoupling protein 2 (mitochondrial, proton carrier)	Ucp2
PrimePCR Reverse Transcription Control Assay	RT

Figure 1: mice, mitoplast purification and attached patch clamp. (A) PCR analysis of tail clip genotyping of WT, heterozygous, and *Kcnt2*$^{-/-}$, mice. 822 bp amplicon expected for WT allele and 547 bp expected for knockout allele. **(B)** Custom 3D printed micro chamber for patch-clamp of mitoplasts with computer model (left) and final product (right). Stereolithography file is deposited at: https://3dprint.nih.gov/discover/3dpx-008253. **(C)** Schematic depicting mitochondrial purification, mitoplast preparation, attached patch and excised patch configuration. **(D)** Western blot of proteins from different cellular fractions during mitochondrial purification. (Homog: homogenate, Cyto: cytosol, Memb: crude membrane, Crude Mito: mitochondrial enriched fraction, ER+Mito: upper band following Percoll™, Pure Mito: lower band following Percoll™). PMNKA: plasma membrane Na+/K+-ATPase, SERCA: sarco-endoplasmic reticulum Ca2+-ATPase, VDAC: mitochondrial outer membrane voltage dependent anion channel, SDHA: mitochondrial inner membrane succinate dehydrogenase subunit A. **(E)** Representative recordings from attached patch clamp of WT and *Kcnt2*$^{-/-}$ mitoplasts, with perfusion of 150 mM KCl (white), after addition of 40 mM NaCl (dark grey), and after addition of 10 µM BT (Black). **(F)** Quantitation of traces normalized to pA/pF and shown as % increase in current at holding potential of 50mV (Same color scheme as **(E)**). Data are means ± SD, from 4-10 independent mitoplast preparations.

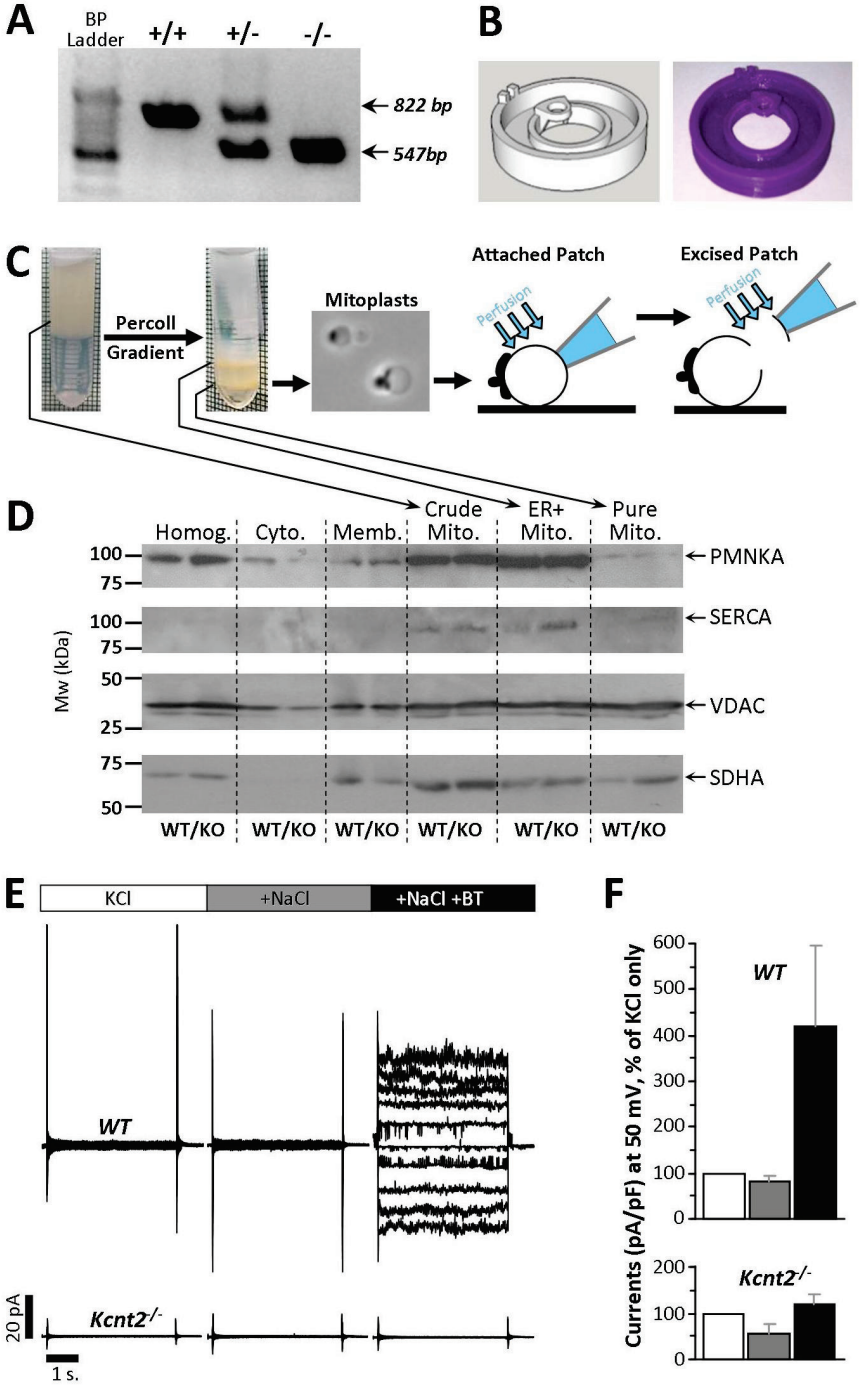

Figure 2: Mitochondria Contain a $K_{Na}1.2$ Channel. (A) Preparations from WT (left) and *Kcnt2*$^{-/-}$ (right) mitoplasts, sorted by channels observed (blue) or no channels observed (white). **(B)** Exclusion of Ca^{2+}-activated (gold) or Li^{+}-activated (light gray) channels. **(C)** Selection of channels activated by Na^{+} and bithionol (BT), with exclusion of channels activated by Na^{+} alone and subsequently blocked by BT (dark gray). For panels B & C, channels carried over to the subsequent screening step are shown in blue. **(D)** Selection of channels with peak conductance matching that reported for $K_{Na}1.2$ (red). **(E)** Example traces of channels observed in WT and *Kcnt2*$^{-/-}$ preparations with a variety of peak conductances (pS, shown in gray inset). Red trace indicates a channel assigned as $K_{Na}1.2$. **(F)** Peak conductance of channels observed from all traces. Color key for panels B-F shown at base of panel. N.B. Channels with conductance >500 pS are omitted for clarity. **(G)** Example of 2 s. recordings from three $K_{Na}1.2$ channels observed in WT mitoplasts (i.e., red points in Figure 1F) at -40 mV holding potential. Current scale bar indicated at left. Closed states are indicated by gray dashed line labeled "C". **(H)** Channel current vs. voltage plot of peak unitary conductances of all $K_{Na}1.2$ channels from WT mitoplast recordings. Average slope conductance was 138±1 pS**.**

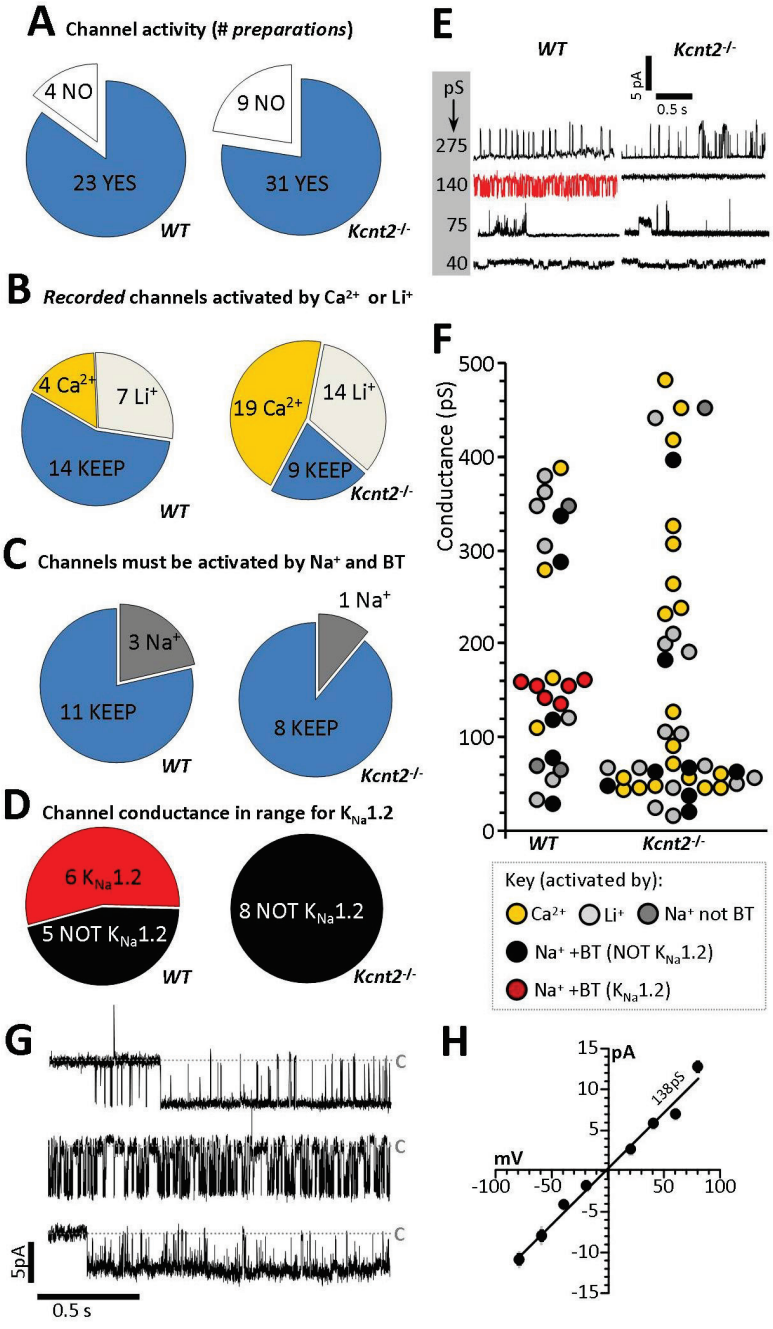

Figure 3: Single Channel Characteristics of Mitochondrial $K_{Na}1.2$. (A) Expanded traces from recordings of patches containing five mitochondrial $K_{Na}1.2$ channels (holding potential -20mV) and a time-expanded trace for the region highlighted by the gray bar in the trace above. Gray dotted lines represent closed ("C") and multiple open (O_1, O_2, O_3, etc.) states. **(B)** Traces from a single $K_{Na}1.2$ channel, at holding potentials of 40mV to -80mV. **(C)** Channel open probability plot from the channel shown in panel B. **(D)** Representative trace of a recording with two channels on a compressed time scale (upper) and a time-expanded trace for the region highlighted by the gray bar in the trace above, showing multiple subconductance states within the channel peak conductance (O_{S1}, O_{S2}, O_{S3} etc.). **(E)** Current Voltage relationship of all six mito-$K_{Na}1.2$ channels showing average current at each holding potential. The decreased slope conductance (compared to Figure 2H showing peak unitary conductance) indicates that subconductances averaging 75 pS dominate the average current during the recordings. **(F)** 45 s continuous trace of a single channel. Gray areas indicate portions of each trace (right) which are repeated (left) on the next line. Closed states are indicated by gray dashed line labeled "C". **(G)** Log binned channel closed (sky blue) and open (salmon) dwell-time peaks and frequency of closed dwell times plotted against their duration. Table insert shows calculated Area and time constant (τ) values.

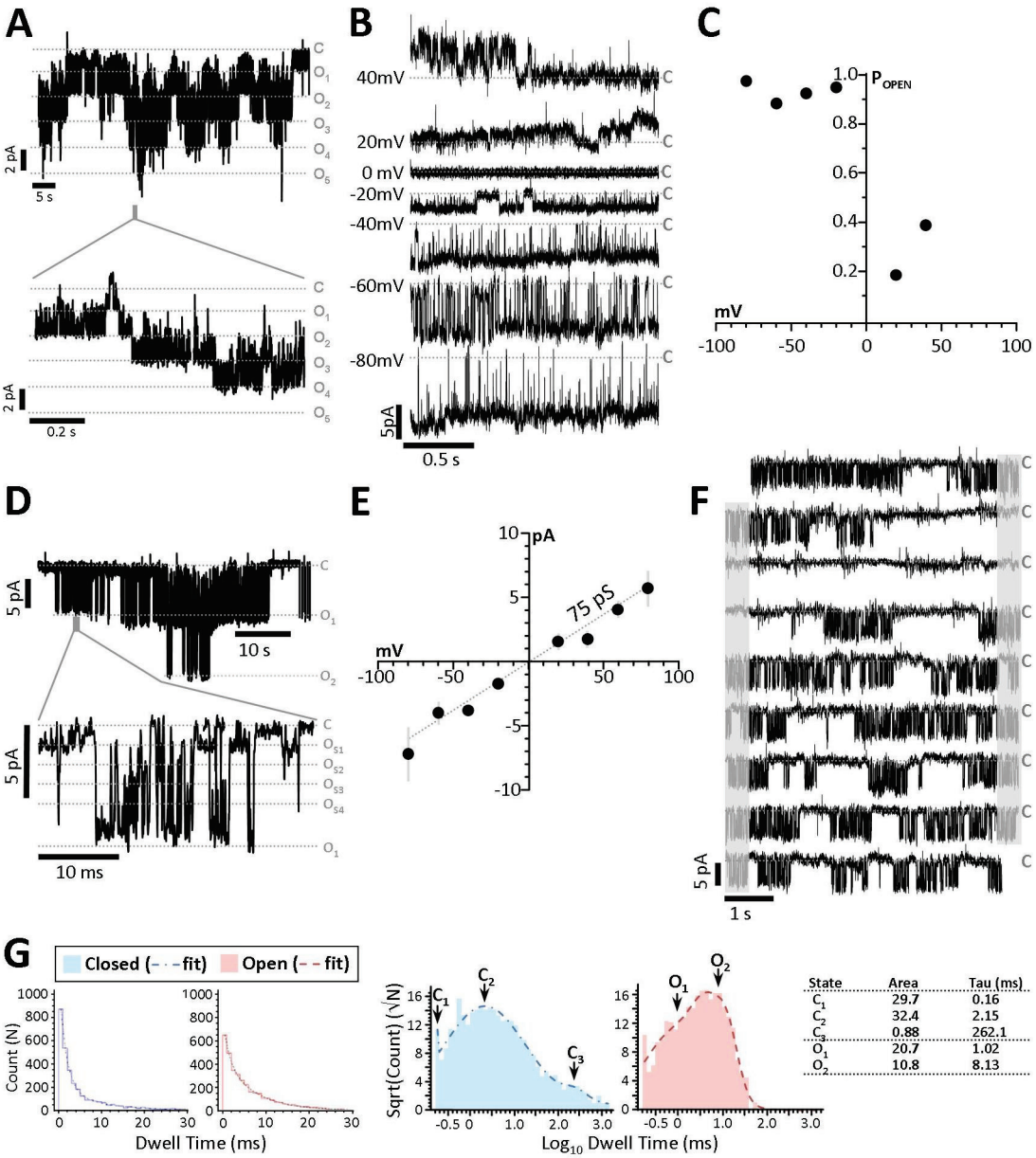

Figure 4: Cardiomyocyte Bioenergetics and Mitochondrial Ultrastructure. (A) Representative images of isolated cardiomyoctes from WT and *Kcnt2*$^{-/-}$ hearts. Black scale bar is 100 µm. **(B)** Oxygen consumption rate (OCR) of isolated cardiomyocytes measured in XF96 Seahorse Analyzer, with addition of oligomycin (1µg/ml) and either 2.5 µM bithionol (K_{Na} opener) or 500 nM FCCP (mitochondrial uncoupler). Statistics were measured using 2-way ANOVA with Bonferroni correction and post-hoc *t*-test. Bars with the same symbol are significantly different from each other ($p<0.05$). Data are means±SEM, N=4-5. **(C)** Western blots from WT and *Kcnt2*$^{-/-}$ heart homogenates showing levels of mitochondrial proteins (SDHA, ICDH, CypD and EFTA), and Ponceau stain loading control. **(D)** Representative transmission electron microscope (EM) images from fixed heart slices. For each genotype, lower left panels show inset boxes at higher magnification. Both white scale bars = 1 µm. Right panels show increased magnification of single mitochondria from WT and *Kcnt2*$^{-/-}$ mice with mitochondrial ultrastructure visible (i.e., cristae folds, outer and inner membrane contacts). Black scale bar 200 nm. **(E)** Binned histogram of mitochondrial area or mitochondrial density, obtained from analysis of EM images using ImageJ software. Data are means±SEM for each bin, N=3-4. **(F)** Form-factor/aspect-ratio scatter plot. Values in panels E and F were obtained from N=1054/789 mitochondria, from 17/14 fields of view, from 4/3 hearts, of WT/*Kcnt2*$^{-/-}$.

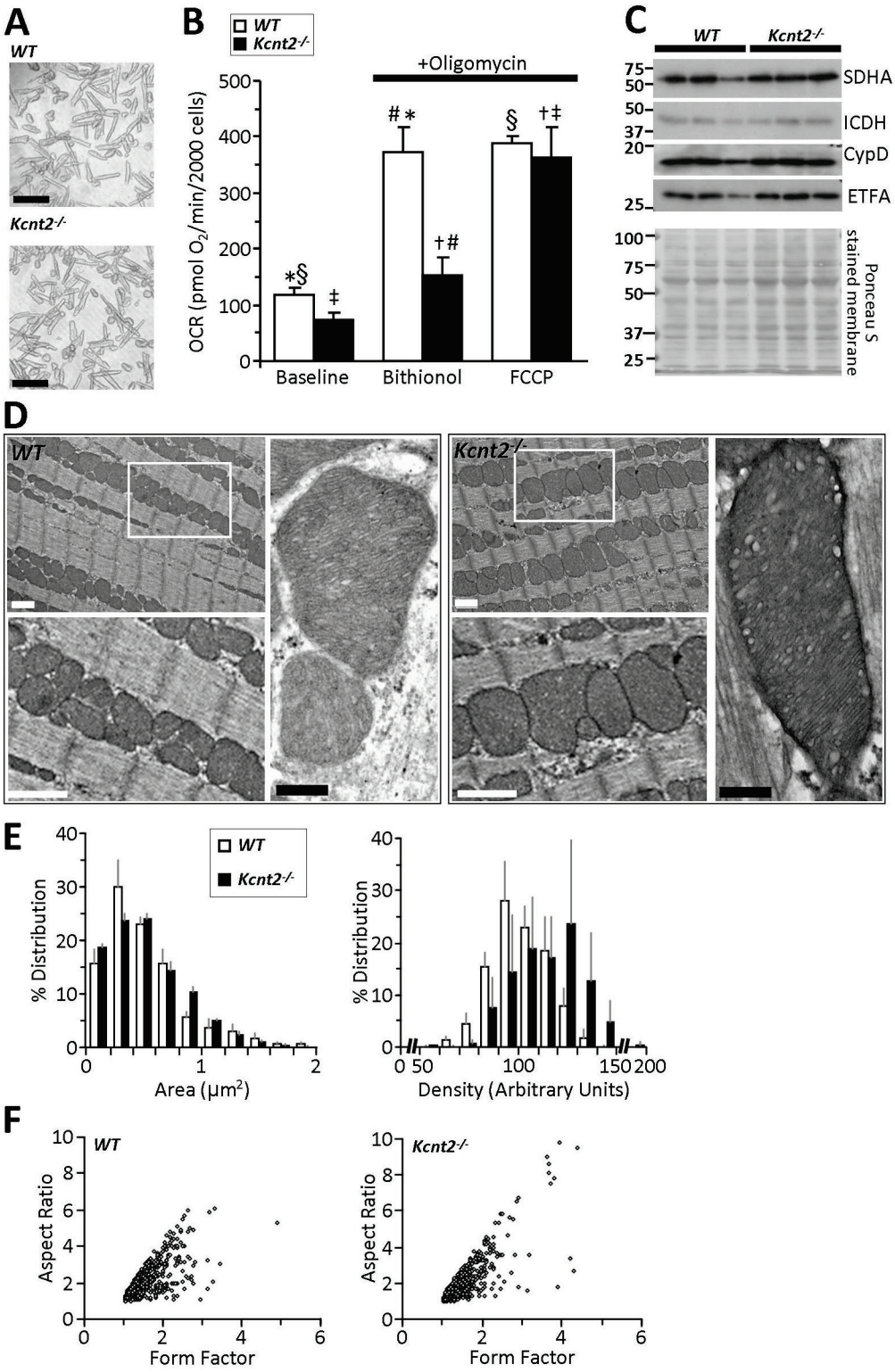

Figure 5: $K_{Na}1.2$ Loss Impacts Cardiac Metabolic Substrate Choice under Stress. (A) Representative Seahorse XF oxygen consumption rate (OCR) traces of isolated WT or *Kcnt2*$^{-/-}$ cardiomyocytes, incubated in the presence of different metabolic substrates: glucose (red), palmitate (blue), glucose + palmitate (purple). Data from a single XF plate are shown (means ± SD of 12 wells per substrate or genotype). Timeline above traces shows OCR was measured at baseline, then with addition of the ATP synthase inhibitor oligomycin (1 µg/ml) plus the mitochondrial uncoupler FCCP (500 nM), and finally with the mitochondrial complex III inhibitor antimycin A (5 µM). **(B)** Group OCR averages of baseline (B) and FCCP-uncoupled (F) cardiomyocytes under substrate conditions as defined above. Statistics were measured using 2-way ANOVA with Bonferroni correction and post-hoc *t*-test. Data are means ± SEM, for N=4 *Kcnt2*$^{-/-}$ or 5 WT, independent cardiomyocyte preparations. Bars with the same symbol are significantly different from each other ($p<0.05$). **(C)** Respiratory reserve (RR) capacity calculated from the data in panel B (i.e., uncoupled minus baseline OCR). Means ± SEM, N=4-5, *$p<0.05$ between genotypes. Color key for metabolic substrates used in all panels is shown to the right of panel C. **(D)** Oxygen consumption rates (OCR) of WT and *Kcnt2*$^{-/-}$ cardiomyocytes metabolizing different substrates: lactate (lime), glutamine (gold), galactose (rose), or pyruvate (copper). Empty bars = baseline (B), Filled bars = FCCP uncoupled (F). Data are means ± SEM from 4-5 independent cardiomyocyte preparations.

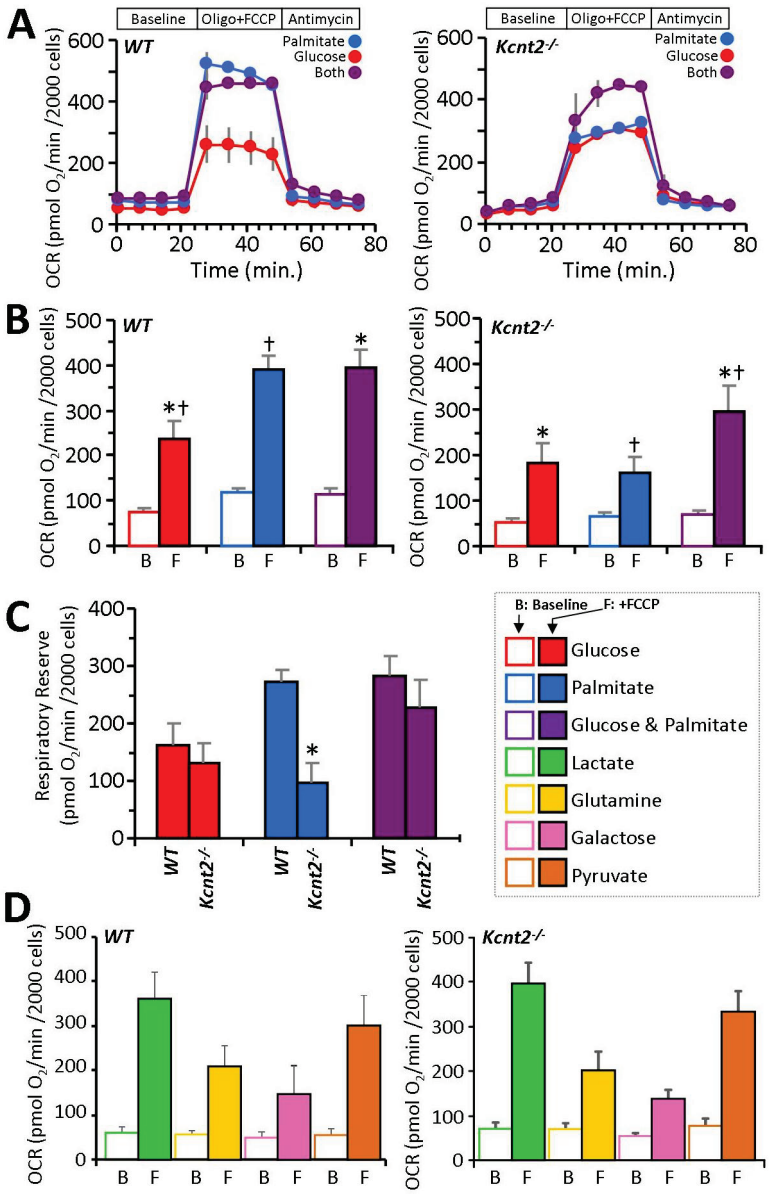

Figure 6: (A) Cardiac function data (heart rate x pressure product, RPP) for isolated perfused hearts from WT or *Kcnt2*$^{-/-}$ mice, perfused with Krebs-Henseleit (KH) buffer containing palmitate as the sole metabolic substrate. Bar below the trace indicates duration of 100 nM isoproterenol infusion. Graph shows RPP as a % of the average baseline value for 1 min before isoproterenol infusion. Inset bar graph shows comparison of the peak response to isoproterenol under this substrate condition (palmitate only, blue). Adjacent inset (right) shows the peak response to isoproterenol from a separate series of perfusions in which the KH buffer contained both palmitate and glucose as substrates (purple). Data are means ± SEM, N=7, *p<0.05 between genotypes. **(B)** EKG parameters obtained *in-vivo* from avertin-anesthetized WT and *Kcnt2*$^{-/-}$ mice. R-R' = distance between R waves of each beat (i.e., 1/HR), P = p-wave duration. P-R = interval between P and R waves. QRS_1 & QRS_2 = diameter of QRS complex (different calculation algorithms). Q-T = interval between Q and peak of T wave. Q-T_{max} = interval between Q and end of T wave. Q-T_{corr} = QT interval corrected for heart rate). Data are ± SD, N=4-5 animals.

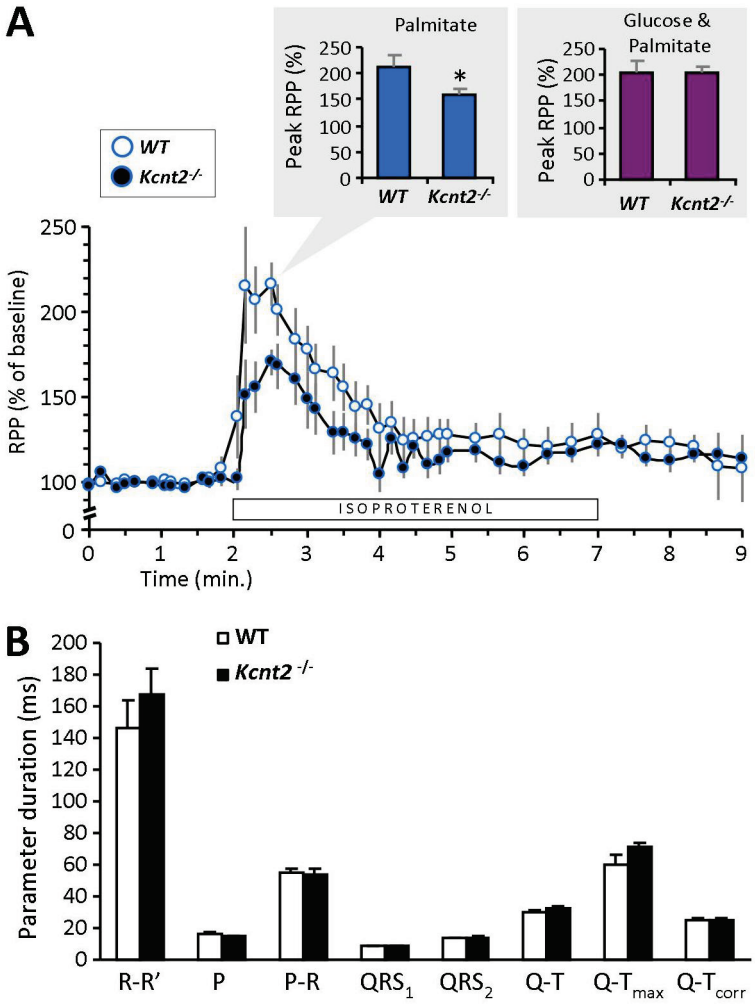

Figure 7: Loss of $K_{Na}1.2$ Impacts Whole Body Metabolic Phenotype. (A) Body weights of WT and *Kcnt2*$^{-/-}$ mice from weaning (3 weeks) to 25 weeks of age. Data are means ± SD, N=12. **(B)** Representative DEXA images from WT and *Kcnt2*$^{-/-}$ mice. **(C)** Percent body fat measured by DEXA scan of WT (white symbols) and *Kcnt2*$^{-/-}$ (black symbols) littermates (pairs are indicated as data points connected by lines), N=14. *p<0.05 between genotypes by paired *t*-test. **(D)** Blood glucose levels measured in WT and *Kcnt2*$^{-/-}$ mice at baseline (5 PM, Fed) and following a 15 hr fast (8 AM, Fasted). Data are means ± SD, N=3. *p<0.05 between fed and fasted state within a genotype. ‡p<0.05 between genotypes at the same time point.

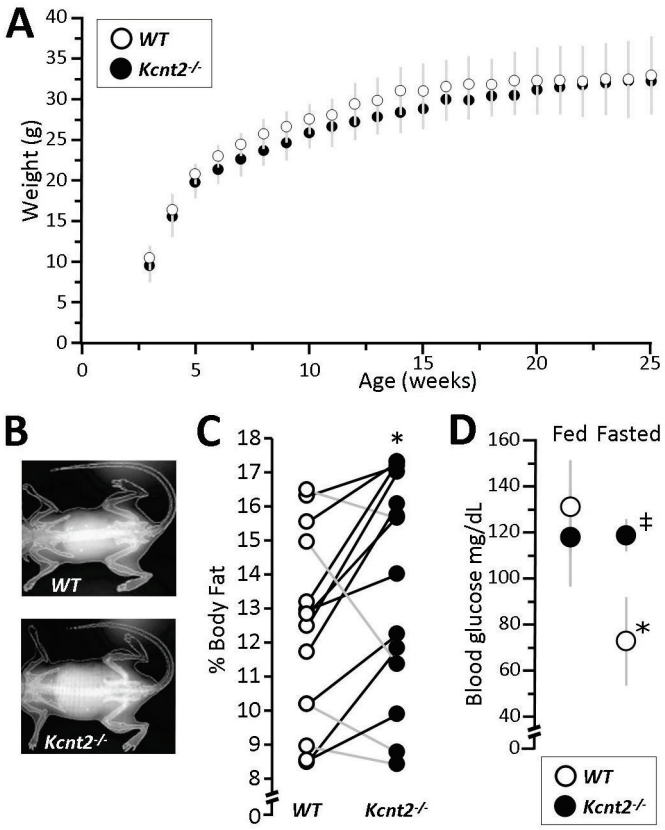

Figure 8: Cardiac Expression Profiling and Metabolomics. (A) qPCR Ct values for 27 metabolically important genes (see Table 1), in WT and *Kcnt2*$^{-/-}$ hearts. N=3 independent RNA preparations per genotype. Data are means, errors are omitted for clarity. **(B)** WT and *Kcnt2*$^{-/-}$ hearts were perfused with KH buffer containing palmitate plus glucose, and freeze-clamped for metabolomic analysis by LC-MS/MS. Graph shows principle component analysis of 501 cardiac metabolites. The first and second principal components contributed 86.7% of the overall metabolic character. Shaded ovals overlaying the graph indicate 95% confidence intervals for WT (lime) and *Kcnt2*$^{-/-}$ (salmon pink) samples. **(C)** Volcano plot of the metabolic profile of *Kcnt2*$^{-/-}$ vs. WT hearts. Axes show -Log$_{10}$(p-value) vs. Log$_{10}$(fold change). Dashed lines show p=0.05 cut off (y axis) and 1.5-fold change cut off (x-axis). Each point represents a single metabolite, and data for each point are means from N=7 hearts. Errors are omitted for clarity. Metabolites passing fold-change and p-value criteria are highlighted red. Additional metabolites discussed in the text are highlighted blue.